



# Interplay of stripe and double- $Q$ magnetism with superconductivity in $\text{Ba}_{1-x}\text{K}_x\text{Fe}_2\text{As}_2$ under the influence of magnetic fields

K. Willa <sup>1,\*</sup>, R. Willa <sup>2</sup>, F. Hardy,<sup>1</sup> L. Wang,<sup>1</sup> P. Schweiss,<sup>1</sup> T. Wolf,<sup>1</sup> and C. Meingast<sup>1</sup>

<sup>1</sup>*Institute for Quantum Materials and Technologies, Karlsruhe Institute of Technology, D-76021 Karlsruhe, Germany*

<sup>2</sup>*Institute for Condensed Matter Theory, Karlsruhe Institute of Technology, D-76131 Karlsruhe, Germany*



(Received 1 December 2022; revised 24 May 2023; accepted 22 June 2023; published 3 August 2023)

At  $x \approx 0.25$   $\text{Ba}_{1-x}\text{K}_x\text{Fe}_2\text{As}_2$  undergoes a novel first-order transition from a fourfold symmetric double- $Q$  magnetic phase to a twofold symmetric single- $Q$  phase, which was argued to occur simultaneously with the onset of superconductivity [Böhmer *et al.*, *Nat. Commun.* **6**, 7911 (2015)]. Here, by applying magnetic fields up to 10 T, we investigate in more detail the interplay of superconductivity with this magnetostructural transition using a combination of high-resolution thermal-expansion and heat-capacity measurements. We find that a magnetic field suppresses the reentrance of the single- $Q$  orthorhombic phase more strongly than the superconducting transition, resulting in a splitting of the zero-field first-order transition. The suppression rate of the orthorhombic reentrance transition is stronger for out-of-plane than for in-plane fields and scales with the anisotropy of the superconducting state. These effects are captured within a phenomenological Ginzburg-Landau model, strongly suggesting that the suppression of the reentrant orthorhombic single- $Q$  phase is primarily linked to the field-induced weakening of the superconducting order. Not captured by this model is, however, a strong reduction in the orthorhombic distortion for out-of-plane fields, which deserves further theoretical attention.

DOI: [10.1103/PhysRevB.108.054504](https://doi.org/10.1103/PhysRevB.108.054504)

## I. INTRODUCTION

The coexistence of superconductivity and magnetism as well as their competition for phase space is a recurring characteristic of iron-based superconductors [1,2]. Superconductivity emerges when the prevailing stripe-type antiferromagnetic spin density wave (SDW) is suppressed by either hole/electron doping or pressure [3–5]. This SDW state is accompanied by an orthorhombic distortion of the lattice which occurs simultaneously or sometimes precedes it in the form of a vestigial nematic transition. Moreover, careful investigations of hole-doped systems, including  $\text{Ba}_{1-x}\text{Na}_x\text{Fe}_2\text{As}_2$ ,  $\text{Ba}_{1-x}\text{K}_x\text{Fe}_2\text{As}_2$ ,  $\text{Sr}_{1-x}\text{Na}_x\text{Fe}_2\text{As}_2$ , and  $\text{Ca}_{1-x}\text{Na}_x\text{Fe}_2\text{As}_2$ , have revealed a plethora of competing new electronic phases near the transition region between stripe antiferromagnetism ( $C_2$ ) and superconductivity. In particular a tetragonal ( $C_4$ ) magnetic phase was discovered in a narrow doping region [6–10]. Neutron studies [11,12] showed that in this magnetically ordered  $C_4$  phase, the moments flip from in plane to out of plane, and Mössbauer studies and Muon spin rotation measurements [13,14] revealed a double- $Q$  order, in which only every other Fe atom carries a magnetic moment. According to the classification of possible double- $Q$  magnetic orders (including hedgehog and loop spin-vortex crystals; see Ref. [15]), this finding is consistent with the so-called spin-charge density wave. In the case of  $\text{Ba}_{1-x}\text{K}_x\text{Fe}_2\text{As}_2$ , initial studies [16–19] did not find the small doping region where the double- $Q$   $C_4$  phase occurs, which was only later revealed upon closer investigation [7] [see Fig. 1(c)]. In contrast to  $\text{Ba}_{1-x}\text{Na}_x\text{Fe}_2\text{As}_2$  and  $\text{Sr}_{1-x}\text{Na}_x\text{Fe}_2\text{As}_2$  [8,10,20], the  $C_4$  phase in  $\text{Ba}_{1-x}\text{K}_x\text{Fe}_2\text{As}_2$  does not extend to zero

temperature; rather superconductivity surprisingly drives the system back to a single- $Q$  orthorhombic magnetic phase [7,21]. Böhmer *et al.* proposed that this was due to the higher electronic entropy available for superconductivity in the single- $Q$  phase compared to the double- $Q$  phase.

Here, by applying magnetic fields up to 10 T, we investigate in more detail the interplay of superconductivity with this magnetostructural transition using a combination of high-resolution thermal-expansion and heat-capacity measurements. We find that a magnetic field suppresses the reentrance of the single- $Q$  orthorhombic phase more strongly than the superconducting transition, resulting in a splitting of the zero-field first-order transition. The suppression rate of the orthorhombic reentrance transition, which remains first order, is stronger for out-of-plane fields than for in-plane fields and scales with the anisotropy of the superconducting state. These effects are captured within a phenomenological Ginzburg-Landau model, strongly suggesting that the suppression of the reentrant orthorhombic magnetic phase is primarily linked to the field-induced weakening of the superconducting order. Not captured by this model is, however, the strong reduction in the orthorhombic distortion for out-of-plane fields, which deserves further theoretical attention.

## II. EXPERIMENTAL DETAILS

Heat-capacity and thermal-expansion measurements were made on two platelet-shaped single crystals of  $\text{Ba}_{1-x}\text{K}_x\text{Fe}_2\text{As}_2$  ( $x \approx 0.24$ ) with masses of 2.63 mg (sample A) and 1.93 mg (sample B) and in-plane dimensions of  $2.1 \times 2.6 \text{ mm}^2$  (sample A). The samples were grown by a self-flux technique [7] and subsequently stored in a glove box in Ar atmosphere. Both crystals are from the same batch as in Ref. [7],

\*kristin.willa@kit.edu

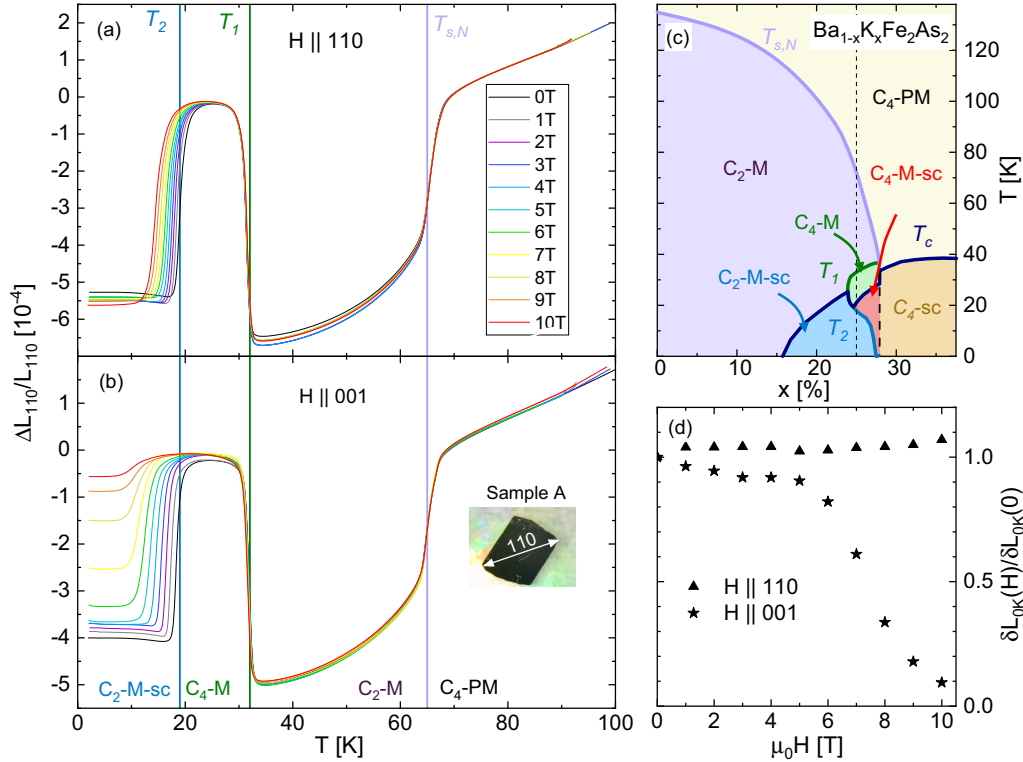


FIG. 1. Temperature dependence of the thermal expansion  $\Delta L/L$  of  $\text{Ba}_{1-x}\text{K}_x\text{Fe}_2\text{As}_2$  measured along the [110] direction in different external magnetic fields for (a)  $H \parallel [110]$  and for (b)  $H \parallel [001]$ . The discontinuities in  $\Delta L/L$  mark the transitions between the  $C_2$  and  $C_4$  phases, as indicated at the bottom. (c) Phase diagram of  $\text{Ba}_{1-x}\text{K}_x\text{Fe}_2\text{As}_2$  for  $0 < x < 0.3$  [7], showing the narrow doping region in which a  $C_4$  phase is observed. (d) The extrapolated magnetic field dependent step height  $\delta L_{0K}(H)/\delta L_{0K}(0)$  as extracted from the thermal expansion measurements.

where more details about the crystal synthesis are provided. Thermal-expansion measurements were performed on sample A in a home-made high-resolution capacitive dilatometer [22]. As demonstrated previously, measurements of the crystal along the  $[110]_T$  direction of the original tetragonal cell ( $C_4$ -PM) produces partial “detwinning” due to the pressure of the springs in the dilatometer cell, giving access to the thermal expansion of the shorter  $b$  axis in the low-temperature stripe phase ( $C_2$ -M) [7,8,23]. Rotating the dilatometry cell allows us to align the magnetic field along both the  $[110]_T$  and  $[001]$  crystal directions. Specific heat measurements were performed on sample B in a 14 T physical property measurement system from Quantum Design with the heat-capacity option.

### III. RESULTS

Figures 1(a) and 1(b) show the relative thermal expansion  $\Delta L_{110}/L_{110}$  of sample A for fields applied parallel to the  $[110]_T$  and  $[001]$  directions, respectively. In zero field, a pronounced reduction in  $\Delta L_{110}/L_{110}$  occurs at  $T_{s,N} = 65$  K, indicative of the transition from the paramagnetic tetragonal state to the  $C_2$  magnetic stripe phase. At lower temperatures, a switching back of  $\Delta L_{110}/L_{110}$  is observed at  $T_1 = 32$  K, where the system enters the double- $Q$  magnetic phase ( $C_4$ -M) that restores tetragonal symmetry, followed by another sudden reduction at  $T_2 = 19$  K, marking the simultaneous reentrance of stripe magnetism and the emergence of superconductivity. Application of an external magnetic field of up to 10 T does

not affect the magnetic transitions at  $T_{s,N}$  and  $T_1$  for either field direction, indicative of a very robust magnetism. The locus of these first-order phase transitions and the determined K concentration of sample A are in good agreement with the reported  $(x, T)$  phase diagram of Ref. [7], which is schematically reproduced in Fig. 1(c) (dashed line). The reduced value of  $\Delta L_{110}/L_{110}$  for  $T < T_2$  with respect to that from extrapolation from the  $C_2$ -M stripe phase indicates, however, that superconductivity, which favors the single- $Q$  stripe phase over the double- $Q$  phase, still competes with the former [24]. In contrast to the transitions at  $T_{s,N}$  and  $T_1$ , a clear shift of  $T_2(H)$  towards lower temperature is observed with increasing field for both field orientations. However, the opposite evolution of  $\Delta L_{110}/L_{110}$ , which is an indicator of the orthorhombic distortion, is quite different inside this reentrant  $C_2$  phase for both field directions. Whereas  $\Delta L_{110}/L_{110}(H)$  is slightly enhanced for fields along  $[110]_T$ , it is drastically reduced to  $\approx 10\%$  of its zero-field value for  $\mu_0 H = 10$  T along the  $[001]$  direction, as illustrated in Fig. 1(d), suggesting an almost complete suppression of the reentrant  $C_2$  phase. These opposite behaviors with field orientation cannot be solely accounted for by the reentrance of the stripe phase, and the influence of superconductivity, which emerges concomitantly in zero field, must be considered. In order to gain further insight about the interplay of superconductivity with the reentrant transition, we also measured the heat capacity for both field orientations.

Figures 2(a) and 2(b) show the respective electronic specific heat of sample B for fields applied perpendicular and

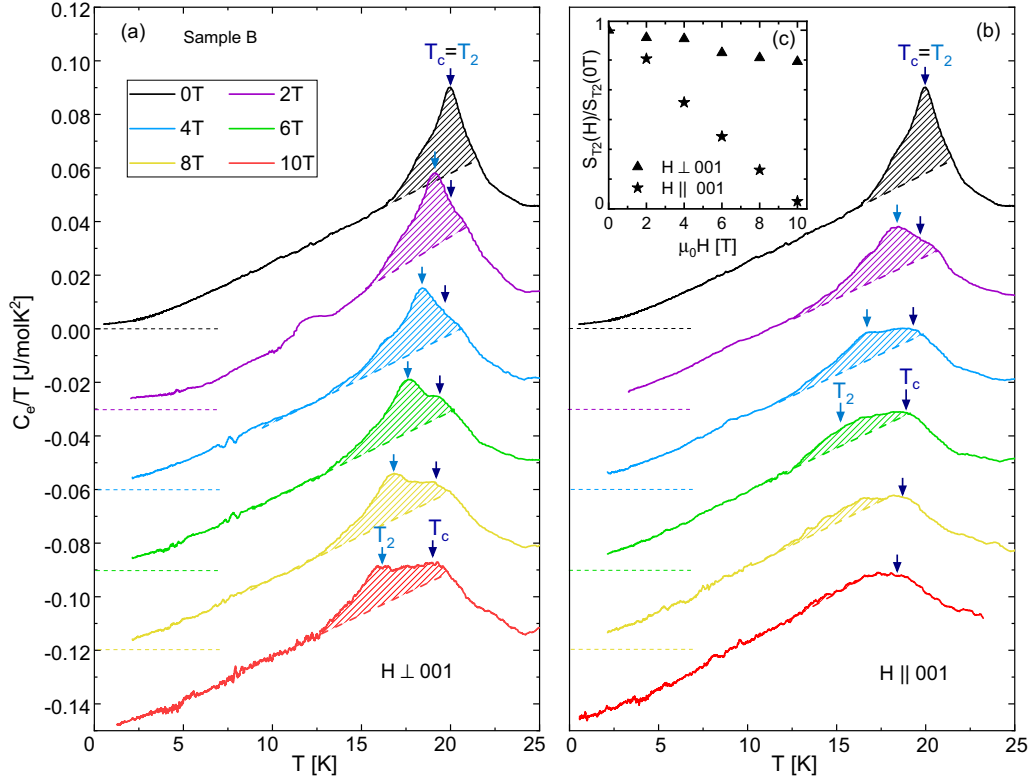


FIG. 2. Temperature dependence of the electronic specific heat for  $\text{Ba}_{1-x}\text{K}_x\text{Fe}_2\text{As}_2$  subject to different applied magnetic fields up to 10 T. To obtain the electronic specific heat we removed the lattice contribution from the measured specific heat. The response to (a) in-plane and (b) out-of-plane magnetic fields. The arrows mark the locations of the superconducting and structural transitions. The shaded region highlights the entropy corresponding to the structural distortion. Curves are shifted vertically by  $-0.03$  J/mol K<sup>2</sup> for every 2 T for clarity; the dashed lines mark the corresponding  $C/T = 0$ . (c) The entropy associated with the  $C_4$ -to- $C_2$  phase transition (equal to the shaded region in  $C/T$ ) normalized by the zero-field entropy.

parallel to the [001] direction, obtained after subtracting a suitable lattice contribution which was obtained through a weighted sum of the individual lattice contributions of  $\text{BaFe}_2\text{As}_2$  and  $\text{KFe}_2\text{As}_2$  (see Ref. [25] for more details). In zero field, a single first-order-like peak at  $T_c = T_2 = 21$  K confirms that the reentrance into the  $C_2$  stripe phase occurs simultaneously with superconductivity, as observed in Ref. [7]. This is corroborated by the vanishing  $C_e/T$  in the  $T \rightarrow 0$  limit, indicative of a fully gapped Fermi surface.

With increasing field, a progressive splitting of the zero-field peak into two distinct anomalies is unambiguously resolved for  $H \perp [001]$ . Here, a broadened mean-field-like anomaly at  $T_c(H)$  marks the transition to the superconducting state (dark blue arrow), followed by a peak at  $T_2(H) < T_c(H)$  where reentrance of the stripe phase takes place (light blue arrow). Thus, our data reveal that with the application of a magnetic field, there are two distinct regions within the superconducting state: one where superconductivity coexists with a single- $Q$  stripe SDW and another one where superconductivity coexists with the double- $Q$  SDW. These regions are separated by the transition at  $T_2(H)$ . In field, the transition at  $T_2$  broadens somewhat but remains first order. To illustrate that, we integrated the electronic specific heat to obtain the electronic entropy in zero field and for 10 T both in plane and out of plane [compare Figs. 3(a) and 3(b)]. For a first-order transition a discontinuity in the entropy would

be expected theoretically, as can be seen in Fig. 3(c) for the simulated entropy curve at  $T_c = T_2$  in zero field. In the experimentally measured curves this discontinuity is broadened, and the transition temperature is rather marked by an inflection point. The theoretically expected behavior is indicated by the dashed lines in Figs. 3(a) and 3(b). For a magnetic field of 10 T applied along the in-plane direction, we observe a change in slope in the entropy at  $T_c$  marking a second-order transition and then a much broader first-order transition, marked again by an inflection point at  $T_2$ . For a magnetic field of 10 T applied along the  $c$  axis, however, only the change in slope at  $T_c$  is visible, and the first-order transition is completely suppressed. This is also consistent with the discontinuity observed in the thermal expansion at  $T_2$ . For  $H \parallel [001]$ , the splitting is also clearly observed [see Fig. 2(b)], but with a more pronounced suppression of  $T_2(H)$ . In contrast to in-plane fields, the peak at  $T_2(H)$  (blue arrow) is rapidly suppressed with increasing  $c$ -axis fields and fades away for  $H > 6$  T. We estimated the entropy associated with this transition by the area between the measured curve and an extrapolation of the quasilinear behavior of the specific heat just below the transition  $T = T_c$  (see shaded areas in Fig. 2). Most prominently, we note that this entropy discontinuity rapidly decreases with increasing field strength for fields along the  $c$  axis while experiencing only moderate changes for in-plane fields. This trend, shown in the inset of Fig. 2(c), is in

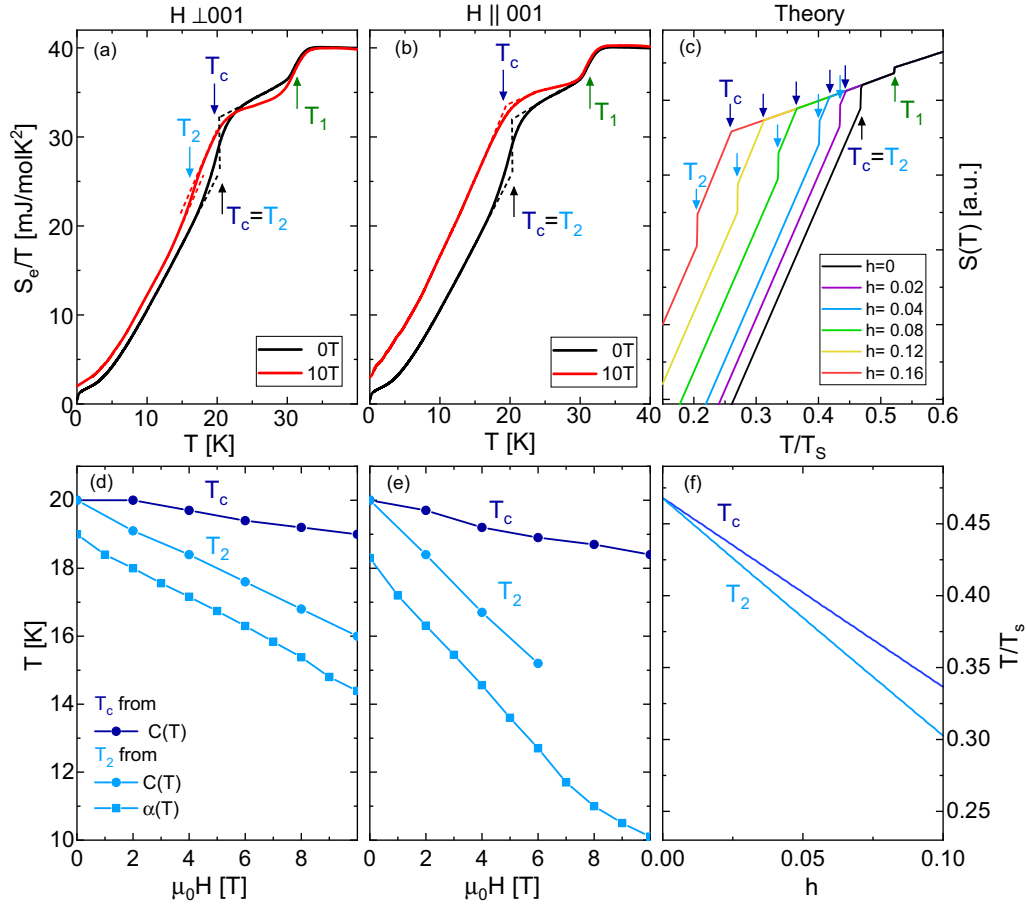


FIG. 3. (a) and (b) The temperature dependence of the electronic entropy in 0 T and for 10 T applied in-plane fields and out-of-plane fields, respectively. (c) The calculated entropy for the theoretical model.  $T_c$ ,  $T_2$ , and  $T_1$  are marked with arrows. The dashed lines guide the eye along the theoretical entropy curve. (d) and (e) The low-temperature phase diagram with transition temperatures  $T_c$  and  $T_2$  taken from specific heat (circles) and thermal expansion (rectangles). (f) Theoretically calculated phase boundary.

line with the field dependence of the orthorhombic distortion, as inferred from our thermal-expansion data [Fig. 1(d)]. We note that we do not observe a clear signature at  $T_c$  in the thermal expansion even at 10 T, where there is a clear separation between  $T_2$  and  $T_c$ . This is surprising since, although they are small, clear thermal expansion anomalies at  $T_c$  have been observed in both  $\text{Ba}_{1-x}\text{Na}_x\text{Fe}_2\text{As}_2$  and  $\text{Sr}_{1-x}\text{Na}_x\text{Fe}_2\text{As}_2$  in the double- $Q$  phase [8,10].

#### IV. THEORETICAL MODEL

Multiple theoretical studies [26–29] investigated the interplay between the different possible magnetic ground states in iron-based superconductors. For a qualitative understanding of the physical mechanisms underlying the presently observed magnetic field dependence of the reentrant transition in  $\text{Ba}_{1-x}\text{K}_x\text{Fe}_2\text{As}_2$ , we aim to capture the key observations within a minimal phenomenological model. We start from the treatment proposed by Kang *et al.* [30] and account for the spin-density modulation  $m = m_x e^{i\mathbf{Q}_x \cdot \mathbf{r}} + m_y e^{i\mathbf{Q}_y \cdot \mathbf{r}}$  and the leading  $s_{\pm}$  superconducting pairing state  $\Delta$  [31–33]. The effective theory for the SDW fields  $\mathbf{m}_{x/y} \propto \frac{1}{2} \sum_{\mathbf{k}} c_{\mathbf{k}}^{\dagger} \sigma_{\mathbf{k}+\mathbf{Q}_{x/y}} (m_{x/y} = |\mathbf{m}_{x/y}|)$  is obtained by applying a Hubbard-Stratonovich transformation to decouple the fermion interaction and

subsequently integrating out the fermionic fields. The free energy functional  $\mathcal{F}[m_x, m_y, \Delta] = \mathcal{F}_m + \mathcal{F}_s + \mathcal{F}_{\text{int}}$  consists of a magnetic part,

$$\mathcal{F}_m = \frac{\alpha}{2}(m_x^2 + m_y^2) + \frac{u}{4}(m_x^2 + m_y^2)^2 - \frac{g}{4}(m_x^2 - m_y^2)^2 + \frac{v}{6}(m_x^2 + m_y^2)(m_x^2 - m_y^2)^2 + \frac{\gamma}{6}(m_x^2 + m_y^2)^3, \quad (1)$$

a minimal superconducting contribution,

$$\mathcal{F}_s = \frac{\alpha_s}{2} \Delta^2 + \frac{u_s}{4} \Delta^4, \quad (2)$$

and a mutual interaction,

$$\mathcal{F}_{\text{int}} = \frac{c_1}{2} \Delta^2 (m_x^2 + m_y^2) + 2c_2 \Delta^2 m_x^2 m_y^2. \quad (3)$$

The magnetic sector  $\mathcal{F}_m$  allows for either a  $C_4$  order with  $m_x = m_y$  or two degenerate  $C_2$  orders with  $m_x = m$  and  $m_y = 0$  or vice versa. The energy sheets associated with these two possibilities evolve differently upon changing external parameters (temperature, doping) and will trigger first-order transitions whenever they cross. Upon entering the magnetic phase, the term  $-(g/4)(m_x^2 - m_y^2)^2$  favors the  $C_2$  magnetic order for  $g > 0$ . For  $v > 0$  the sixth-order term may tip the balance in favor of the  $C_4$  phase. Consequently,  $v$  seems to be a suitable tuning

parameter to capture the dominant doping dependence. The first interaction term in  $\mathcal{F}_{\text{int}}$  accounts for the competition between superconductivity and magnetism ( $c_1 > 0$ ). The second term ( $c_2 > 0$ ) further enhances the competition of superconductivity with the  $C_4$  magnetic order while being absent within the  $C_2$  magnetic phase. Our model extends that of Kang *et al.* [30] by including an isotropic magnetic field dependence in  $\alpha_s$ . This phenomenological description suffices to capture the main effect while the model can trivially be extended to the anisotropic case. Owing to the magnetic field robustness of the first two magnetic transitions observed in the experiment, we attribute the leading field dependence to the superconducting orbital pair breaking. In addition, the second term in  $\mathcal{F}_{\text{int}}$  provides a clear energetic distinction in the way the two magnetic orders couple to superconductivity. Such an interaction was shown to arise from the coupling of the superconducting  $s_{\pm}$  order to an underlying, yet unfulfilled,  $d$ -wave gap function [30]. Without the coupling to magnetism, the superconducting order defined in Eq. (2) appears at a conventional second-order phase transition. However, a combined superconducting and magnetic (from  $C_4$  to the nearly degenerate  $C_2$  phase) first-order transition can occur. In the model it is the second term in Eq. (1), then, that causes the first-order transition. Physically, this is likely related to the additional electronic entropy available for superconducting pairing in the  $C_2$  phase [7]. More details about the model and the specific parameter values are given in the Appendix. The phase diagram in zero magnetic field [Fig. 4(c)] reproduces well the observation reported in Ref. [7]. Upon cooling, the system first enters the  $C_2$  stripe phase, followed, at low doping, by the onset of superconductivity. Above a critical doping, the  $C_2$  magnetic state undergoes a first-order transition into a tetragonal double- $Q$  magnetic phase which lowers the onset of superconductivity, presumably due to additional gapping of the Fermi surface in the double- $Q$  phase [7]. This lost density of states is recovered when, with the onset of superconductivity, the magnetism switches back to the  $C_2$  stripe phase. At even larger doping levels, the last two transitions appear sequentially, with superconductivity setting in as a second-order transition, followed by a first-order switching to the  $C_2$  magnetic state.

For a fixed doping level, indicated by the dashed line in Fig. 4(c), we calculated the heat capacity and  $|m_x - m_y|(T)$  as a proxy for the orthorhombic lattice distortion. Both quantities associated with our model calculation are shown in Figs. 4(a) and 4(b). In zero magnetic field, we observe the first-order transition into the double- $Q$  charge density wave at  $T_1$ , and then superconductivity drives the system back into a single- $Q$  SDW. This joint transition is well captured by both a  $\delta$  peak and a step in the heat capacity as well as a step in the lattice distortion. In magnetic fields, the transition splits apart, and the system becomes first superconducting [step in  $C(T)$ ] and then orthorhombic [ $\delta$  peak in  $C(T)$ ]. As the lattice distortion is zero in the tetragonal phase, the onset of superconductivity is not captured in  $|m_x - m_y|(T)$ . In our model calculations, we observe a field-induced low-temperature increase in the orthorhombic distortion like that observed in the thermal expansion data for  $H \parallel [100]$  (see Fig. 1). In the model, this can be attributed to the field-induced weakening of the competition between superconductivity and stripe-type magnetism.

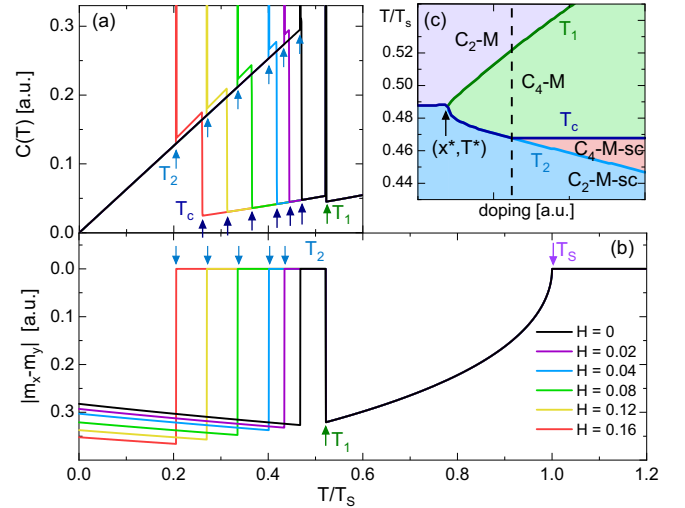


FIG. 4. (a) Calculated heat capacity near the onset of superconductivity for different magnetic field strengths. At zero field, the transition is first order and accompanied by a magnetic switching from the  $C_4$  to the nearly degenerate  $C_2$  stripe order. For sufficiently large fields,  $H \gtrsim 0.02$ , this transition is split into a second-order onset of superconductivity, followed by a first-order magnetic switching. (b) The proxy  $|m_x - m_y|(T)$  of the orthorhombic distortion for different magnetic fields. Transition temperatures are marked with arrows. (c) Close-up of the phase diagram near the tricritical point  $(x^*, T^*)$  where the  $C_2$  and  $C_4$  magnetic phases are degenerate and where superconductivity appears. For larger doping the first-order onset of superconductivity is accompanied by a transition into a  $C_2$  magnetic phase. At even higher doping levels, these two transitions split and allow for a superconducting phase with  $C_4$  magnetic order. The dashed line marks the doping concentration for which the specific heat and orthorhombic distortion are shown in (a) and (b).

## V. DISCUSSION AND CONCLUSION

The transition temperatures inferred from our thermal-expansion and heat-capacity measurements are summarized in the  $(H, T)$  phase diagrams of Figs. 3(d) and 3(e) for  $H \perp [001]$  and  $H \parallel [001]$ , respectively, and are compared to the theoretical phase diagram shown in Fig. 3(f). Here,  $T_2(H)$  is determined experimentally as the position of the maximum in the heat capacity (light blue arrow in Fig. 2) and in the coefficient of linear thermal expansion  $\alpha_{110}(T, H) = 1/L_{110}[(\partial \Delta L_{110})/\partial T]$ . As the peak observed in specific heat broadens considerably with increasing field in the  $[001]$  direction, this criterion is restricted to fields less than 6 T. On the other hand, we determine  $T_c(H)$  as the maximum of the mean-field discontinuity in heat capacity, rather than using an entropy-conserving construction because it is partially obstructed by the nearby broadened transition to the low temperature orthorhombic single- $Q$  state. The small offset in  $T_2(H)$  between the heat capacity (light blue circles) and thermal-expansion data (light blue squares) is likely related to slight variations in K content between the two samples, but this does not affect our discussion since both lines are found to run parallel until 10 T.

We find that  $T_c$  is weakly suppressed for both field orientations, with  $[(\partial T_c)/\partial H] \approx 0.1 \text{ K/T}$  for  $H \perp [001]$  with

the superconducting anisotropy being  $\approx 2$ , a typical value for other Fe-based superconductors as well [34–38]. In contrast, the suppression of  $T_2(H)$  is more pronounced, about a factor of 4 larger than that of  $T_c(H)$ , revealing that a minor weakening of  $T_c(H)$  has a strong impact on the transition into the reentrant single- $Q$  phase. Furthermore, the anisotropy of suppression of  $T_2(H)$  is also close to 2, scaling with the superconducting anisotropy, which strongly suggests that the stripe-phase reentrance is intimately coupled to superconductivity, and by weakening the superconducting order through applied magnetic fields, the reentrance of the low-temperature single- $Q$  SDW is retarded. Although our model does not account for both crystal and magnetic anisotropies, an anisotropic field dependence of  $\alpha_s$  in Eq. (2) matching the experimental superconducting anisotropy immediately reproduces the observed anisotropy of  $T_2(H)$ .

Not reproduced by our minimal model is the contrasting thermal-expansion behavior of the  $b$  orthorhombic axis (see Fig. 1) with respect to the field direction observed deep inside the reentrant orthorhombic single- $Q$  phase. On the one hand, the model reproduces quite well [in Fig. 4(b)] the slight increase in orthorhombicity found for  $H \parallel [110]_T$ . This effect can be understood to result from the well-documented competition between superconductivity and the orthorhombicity in the stripe magnetic phase [24]; that is, the magnetic field suppresses the superconducting order and thereby promotes the coexisting magnetic order. On the other hand, the remarkable rapid disappearance of the orthorhombic distortion and the vanishing entropy discontinuity for  $H \parallel [001]$ , which constitute one of the main results of our study, are quite puzzling and remain to be understood theoretically. A missing ingredient in our model is the accounting for spin-orbit effects, which are clearly important in these materials [12,26,39]. For example, it was found that the  $c$  axis corresponds to the direction of the magnetic moment in the similar  $C_4$  magnetic phase of  $\text{Ba}_{1-x}\text{Na}_x\text{Fe}_2\text{As}_2$  [12].

In conclusion, we studied in detail the magnetic field dependence of the transition from the tetragonal double- $Q$  magnetic phase to the orthorhombic, superconducting single- $Q$  phase in  $\text{Ba}_{1-x}\text{K}_x\text{Fe}_2\text{As}_2$  ( $x \approx 0.25$ ). We reported a splitting of the zero-field first-order transition in applied magnetic fields, with the suppression of the single- $Q$  orthorhombic phase being stronger than the suppression of superconductivity. This can be reproduced by a phenomenological Ginzburg-Landau model, providing evidence that it is the weakening of superconductivity by an applied magnetic field that is responsible for the suppression of the single- $Q$  orthorhombic phase. The suppression rate of this transition temperature is stronger for out-of-plane fields than for in-plane fields, showing the same anisotropy as the superconducting state. Additionally, we observed a strong reduction in the orthorhombic distortion for out-of-plane fields that cannot be captured by our model and calls for further theoretical investigations.

TABLE I. Parameters used in the phenomenological model.

$\alpha(\tau)$	$u$	$g$	$v$	$\gamma$	$\alpha_s$	$u_s$	$\tau_c(H)$	$c_1$	$c_2$
$\tau - 1$	4	0.5	$x$	4	$\tau - \tau_c$	1	$0.6 - H$	1	0.2

## ACKNOWLEDGMENTS

We acknowledge stimulating discussions with R. Fernandes. K.W. acknowledges support from the Swiss National Science Foundation through the Postdoc.Mobility program. We acknowledge support from the Deutsche Forschungsgemeinschaft (DFG; German Research Foundation) under CRC/TRR 288. R.W. was supported by the German Research Foundation (DFG) through CRC TRR 288 ElastoQMat, project A07.

## APPENDIX: THEORETICAL MODEL

The phenomenology in  $\text{Ba}_{1-x}\text{K}_x\text{Fe}_2\text{As}_2$  is well captured by the Ginzburg-Landau free energy density  $\mathcal{F} = \mathcal{F}_m + \mathcal{F}_s + \mathcal{F}_{\text{int}}$ , as specified in Eqs. (1)–(3). The magnetic texture realizes either a double- $Q$  spin-density wave order ( $|m_x| = |m_y|$ ) that preserves the  $C_4$  symmetry or a single- $Q$  stripe magnetic order ( $m_x m_y = 0$ ) lowering the in-plane rotational symmetry to  $C_2$ . These two possibilities define distinct energy manifolds, between which first-order transitions can occur. Once superconductivity appears, the leading interaction term in  $\mathcal{F}_{\text{int}}$  only mildly affects the energetics between the two magnetic sectors. The next order term  $\propto c_2$ , on the other hand, strongly differentiates between the  $C_4$  order (where it vanishes) and the  $C_2$  phase.

In order to study this model system we limit ourselves to a simple description in which the temperature dependence is limited to the two mass terms,  $\alpha$  and  $\alpha_s$ . By identifying  $v = \nu x$ , with  $\nu \approx 32$ , we attribute the dominant doping dependence  $x$  to the term dictating the relative energetics of the magnetic phases. Experimentally, the magnetic field dependence of  $\text{Ba}_{1-x}\text{K}_x\text{Fe}_2\text{As}_2$  can, to a large extent, be reduced to the superconducting sector. This motivates our choice of coupling only the phenomenological parameter  $\alpha_s$  to the magnetic field  $H$ . The specific choice of parameters is provided in Table I.

Within our model, the calorimetric data can be deduced from  $C = T \partial^2 E / \partial T^2$ , where  $E(T)$  is the system's energy at a given temperature  $T$ . Furthermore, the coupling of the stripe spin-density state ( $|m_x - m_y| \neq 0$ ) to the elastic degrees of freedom will result in a length change of the specimen. We anticipate that  $\delta L/L \propto |m_x - m_y|$  and use the latter as a proxy for the former.

Note that the orientation of the moments in the different magnetic phases is susceptible to change due to crystal field effects. This aspect is not accounted for within the proposed model. In particular, it is not capable of resolving the field-direction dependence at low temperature (see Fig. 1).

[1] J. Lorenzana, G. Seibold, C. Ortix, and M. Grilli, *Phys. Rev. Lett.* **101**, 186402 (2008).

[2] R. M. Fernandes, A. V. Chubukov, and J. Schmalian, *Nat. Phys.* **10**, 97 (2014).

- [3] J. Paglione and R. L. Greene, *Nat. Phys.* **6**, 645 (2010).
- [4] M. Rotter, M. Pangerl, M. Tegel, and D. Johrendt, *Angew. Chem., Int. Ed.* **47**, 7949 (2008).
- [5] M. S. Torikachvili, S. L. Bud'ko, N. Ni, and P. C. Canfield, *Phys. Rev. Lett.* **101**, 057006 (2008).
- [6] S. Avci, O. Chmaissem, J. M. Allred, S. Rosenkranz, I. Eremin, A. V. Chubukov, D. E. Bugaris, D. Y. Chung, M. G. Kanatzidis, J. P. Castellán, J. A. Schlueter, H. Claus, D. D. Khalyavin, P. Manuel, A. Daoud-Aladine, and R. Osborn, *Nat. Commun.* **5**, 3845 (2014).
- [7] A. E. Böhmer, F. Hardy, L. Wang, T. Wolf, P. Schweiss, and C. Meingast, *Nat. Commun.* **6**, 7911 (2015).
- [8] L. Wang, F. Hardy, A. E. Böhmer, T. Wolf, P. Schweiss, and C. Meingast, *Phys. Rev. B* **93**, 014514 (2016).
- [9] K. M. Taddei, J. M. Allred, D. E. Bugaris, S. H. Lapidus, M. J. Krogstad, H. Claus, D. Y. Chung, M. G. Kanatzidis, R. Osborn, S. Rosenkranz, and O. Chmaissem, *Phys. Rev. B* **95**, 064508 (2017).
- [10] L. Wang, M. He, D. D. Scherer, F. Hardy, P. Schweiss, T. Wolf, M. Merz, B. M. Andersen, and C. Meingast, *J. Phys. Soc. Jpn.* **88**, 104710 (2019).
- [11] J. M. Allred, S. Avci, D. Y. Chung, H. Claus, D. D. Khalyavin, P. Manuel, K. M. Taddei, M. G. Kanatzidis, S. Rosenkranz, R. Osborn, and O. Chmaissem, *Phys. Rev. B* **92**, 094515 (2015).
- [12] F. Waßer, A. Schneidewind, Y. Sidis, S. Wurmehl, S. Aswartham, B. Büchner, and M. Braden, *Phys. Rev. B* **91**, 060505 (2015).
- [13] B. P. Mallett, Y. G. Pashkevich, A. Gusev, T. Wolf, and C. Bernhard, *Europhys. Lett.* **111**, 57001 (2015).
- [14] J. M. Allred, K. M. Taddei, D. E. Bugaris, M. J. Krogstad, S. H. Lapidus, D. Y. Chung, H. Claus, M. G. Kanatzidis, D. E. Brown, J. Kang, R. M. Fernandes, I. Eremin, S. Rosenkranz, O. Chmaissem, and R. Osborn, *Nat. Phys.* **12**, 493 (2016).
- [15] W. R. Meier, Q. P. Ding, A. Kreyssig, S. L. Bud'ko, A. Sapkota, K. Kothapalli, V. Borisov, R. Valentí, C. D. Batista, P. P. Orth, R. M. Fernandes, A. I. Goldman, Y. Furukawa, A. E. Böhmer, and P. C. Canfield, *npj Quantum Mater.* **3**, 5 (2018).
- [16] E. Hassinger, G. Gredat, F. Valade, S. R. De Cotret, A. Juneau-Fecteau, J. P. Reid, H. Kim, M. A. Tanatar, R. Prozorov, B. Shen, H. H. Wen, N. Doiron-Leyraud, and L. Taillefer, *Phys. Rev. B* **86**, 140502 (2012).
- [17] S. Avci, O. Chmaissem, E. A. Goremychkin, S. Rosenkranz, J. P. Castellán, D. Y. Chung, I. S. Todorov, J. A. Schlueter, H. Claus, M. G. Kanatzidis, A. Daoud-Aladine, D. Khalyavin, and R. Osborn, *Phys. Rev. B* **83**, 172503 (2011).
- [18] S. Avci, O. Chmaissem, D. Y. Chung, S. Rosenkranz, E. A. Goremychkin, J. P. Castellán, I. S. Todorov, J. A. Schlueter, H. Claus, A. Daoud-Aladine, D. D. Khalyavin, M. G. Kanatzidis, and R. Osborn, *Phys. Rev. B* **85**, 184507 (2012).
- [19] M. A. Tanatar, W. E. Straszheim, H. Kim, J. Murphy, N. Spyrison, E. C. Blomberg, K. Cho, J. P. Reid, B. Shen, L. Taillefer, H. H. Wen, and R. Prozorov, *Phys. Rev. B* **89**, 144514 (2014).
- [20] E. Sheveleva, B. Xu, P. Marsik, F. Lyzwa, B. P. Mallett, K. Willa, C. Meingast, T. Wolf, T. Shevtsova, Y. G. Pashkevich, and C. Bernhard, *Phys. Rev. B* **101**, 224515 (2020).
- [21] E. I. Timmons, M. A. Tanatar, K. Willa, S. Teknowijoyo, K. Cho, M. Kończykowski, O. Cavani, Y. Liu, T. A. Lograsso, U. Welp, R. Prozorov, M. Konczykowski, O. Cavani, Y. Liu, T. A. Lograsso, U. Welp, and R. Prozorov, *Phys. Rev. B* **99**, 054518 (2019).
- [22] C. Meingast, B. Blank, H. Bürkle, B. Obst, T. Wolf, H. Wühl, V. Selvamanickam, and K. Salama, *Phys. Rev. B* **41**, 11299 (1990).
- [23] M. He, L. Wang, F. Hardy, L. Xu, T. Wolf, P. Adelman, and C. Meingast, *Phys. Rev. B* **97**, 104107 (2018).
- [24] S. Nandi, M. G. Kim, A. Kreyssig, R. M. Fernandes, D. K. Pratt, A. Thaler, N. Ni, S. L. Bud'ko, P. C. Canfield, J. Schmalian, R. J. McQueeney, and A. I. Goldman, *Phys. Rev. Lett.* **104**, 057006 (2010).
- [25] F. Hardy, A. E. Böhmer, L. de'Medici, M. Capone, G. Giovannetti, R. Eder, L. Wang, M. He, T. Wolf, P. Schweiss, R. Heid, A. Herbig, P. Adelman, R. A. Fisher, and C. Meingast, *Phys. Rev. B* **94**, 205113 (2016).
- [26] M. H. Christensen, J. Kang, B. M. Andersen, I. Eremin, and R. M. Fernandes, *Phys. Rev. B* **92**, 214509 (2015).
- [27] M. H. Christensen, P. P. Orth, B. M. Andersen, and R. M. Fernandes, *Phys. Rev. B* **98**, 014523 (2018).
- [28] M. H. Christensen, D. D. Scherer, P. Kotetes, and B. M. Andersen, *Phys. Rev. B* **96**, 014523 (2017).
- [29] D. D. Scherer and B. M. Andersen, *Phys. Rev. Lett.* **121**, 037205 (2018).
- [30] J. Kang, X. Wang, A. V. Chubukov, and R. M. Fernandes, *Phys. Rev. B* **91**, 121104(R) (2015).
- [31] K. Kuroki, H. Usui, S. Onari, R. Arita, and H. Aoki, *Phys. Rev. B* **79**, 224511 (2009).
- [32] S. Maiti, M. M. Korshunov, T. A. Maier, P. J. Hirschfeld, and A. V. Chubukov, *Phys. Rev. Lett.* **107**, 147002 (2011).
- [33] T. Böhm, A. F. Kemper, B. Moritz, F. Kretschmar, B. Muschler, H. M. Eiter, R. Hackl, T. P. Devereaux, D. J. Scalapino, and H. H. Wen, *Phys. Rev. X* **4**, 041046 (2014).
- [34] M. A. Tanatar, Y. Liu, J. Jaroszynski, J. S. Brooks, T. A. Lograsso, and R. Prozorov, *Phys. Rev. B* **96**, 184511 (2017).
- [35] K. Willa, R. Willa, J.-K. Bao, A. E. Koshelev, D. Y. Chung, M. G. Kanatzidis, W.-K. Kwok, and U. Welp, *Phys. Rev. B* **99**, 180502(R) (2019).
- [36] M. P. Smylie, A. E. Koshelev, K. Willa, R. Willa, W.-K. Kwok, J.-K. Bao, D. Y. Chung, M. G. Kanatzidis, J. Singleton, F. F. Balakirev, H. Hebbeker, P. Niraula, E. Bokari, A. Kayani, and U. Welp, *Phys. Rev. B* **100**, 054507 (2019).
- [37] K. Willa, M. P. Smylie, Y. Simsek, J. K. Bao, D. Y. Chung, M. G. Kanatzidis, W. K. Kwok, and U. Welp, *Phys. Rev. B* **101**, 064508 (2020).
- [38] F. Hardy, L. Doussoulin, T. Klein, M. He, A. Demuer, R. Willa, K. Willa, A. A. Haghighirad, T. Wolf, M. Merz, C. Meingast, and C. Marcenat, *Phys. Rev. Res.* **2**, 033319 (2020).
- [39] C. Liu, P. Bourges, Y. Sidis, T. Xie, G. He, F. Bourdarot, S. Danilkin, H. Ghosh, S. Ghosh, X. Ma, S. Li, Y. Li, and H. Luo, *Phys. Rev. Lett.* **128**, 137003 (2022).